# Session 2A4
# Non-linear Inverse Problems in Electromagnetic Medical Imaging

# Inverse Electromagnetic Scattering Problems for Partially Coated Objects

**F. Cakoni, D. Colton, and P. Monk**
University of Delaware, USA

We consider the three dimensional electromagnetic inverse scattering problem of determining information about a coated object from a knowledge of the electric far field patterns corresponding to time harmonic incident plane waves at fixed frequency. To fix our ideas we consider a anisotropic dielectric obstacle (partially) coated by a thin layer of a highly conducting material, which is modelled by a transmission boundary value problem with conducting transmission condition on the coated part. No a priori assumption is made on the connectivity of the scattering obstacle nor on the extent of the coating, i.e., the object can be either fully coated, partially coated or not coated at all. We present an algorithm for reconstructing the shape of the scattering obstacle together with an estimate of either the surface impedance or surface conductivity. Numerous numerical examples are given showing the efficaciousness of our method.

# A High-order Finite Element Method for Electrical Impedance Tomography

**S. Pursiainen and H. Hakula**
Helsinki University of Technology, Finland

**Abstract**—Electrical impedance tomography (EIT) is a non-invasive imaging technique where a conductivity distribution in a domain is reconstructed from boundary voltage measurements. The voltage data are generated by injecting currents into the domain. This is an ill-conditioned non-linear inverse problem. Small measurement or forward modeling errors can lead to unbounded fluctuations in the reconstructions. A forward model describes the dependence of the noiseless voltage data on the conductivity distribution. The present work focuses on applying the high-order finite element method ($p$-FEM) for forward modeling. In the traditional version of the finite element method ($h$-FEM), the polynomial degree of the element shape functions is relatively low and the discretization error is reduced by increasing the number of elements. In the $p$-version, in contrast, the polynomial degree is increased and the mesh size is kept constant. In many applications of the finite element method the performance of the $p$-version is better than that of the $h$-version. In this work, it is proposed that the $p$-version provides more efficient tool for EIT forward modeling. Numerical results are presented.

## 1. Introduction

The electrical impedance tomography (EIT) problem is to reconstruct an unknown conductivity distribution $\sigma$ in an object $\Omega$ from a set of noisy voltage measurements performed on the boundary $\partial\Omega$ This problem was first introduced in 1980 by Calderón [1]. At the present, EIT has numerous applications. These include detection of tumors from breast tissue [5], measuring brain function [8], imaging of fluid flows in process pipelines [10], and non-destructive testing of materials [13]. For a review on EIT, see Cheney *et al.*, [2].

In the present version of electrical impedance tomography, a current pattern $I = (I_1, I_2, \ldots, I_L)$ is injected into a two dimensional domain $\Omega$ through a set of contact electrodes $e_1$, $e_2$, ..., $e_L$ placed on the boundary $\partial\Omega$. The injected currents induce a potential field u in the domain and a electrode voltages $U = (U_1, U_2, \ldots, U_L)$. The measurement data are gathered by injecting a set of linearly independent current patterns and measuring the corresponding electrode voltages. The conductivity distribution in $\Omega$ is to be reconstructed from these voltage measurements. This is a non-linear ill-conditioned inverse problem: small errors in the measurements or in the forward modeling can produce large errors in the reconstructions.

The focus of this paper is in efficient forward modeling. A forward model describes the dependence of the noiseless voltage data on the conductivity distribution. The complete electrode model by Somersalo et al., [9] and its simulations through the traditional finite element method ($h$-FEM) and the high-order finite element method (p-FEM) are considered. According to the complete electrode model, the potential distribution in the domain and the voltages on the electrodes can be determined by solving an elliptic boundary value problem. Finite element simulation of this forward model has been described by Vauhkonen [12]. In the $h$-version of FEM, the polynomial order $p$ of the element shape functions is relatively low and the discretization error is reduced by decreasing the element size $h$. In the $p$-version, in contrast, the polynomial order is increased and the mesh size is kept constant. Processes where either the mesh is refined or the polynomial degree is increased are called $h-$ and $p$-extensions, respectively. Both extension processes increase the dimension of the finite element space which is denoted by $N$. Combinations of $h-$ and $p$-extensions are called $hp$-extensions ($hp$-FEM). Descriptions of $h-$, $p-$ and $hp$-versions of FEM are given e. g., in a book by Szabo and Babuska [11].

This work presents numerical results on performances of $h-$ and $p$-extensions in finite element simulation of the complete electrode model. The motivation for this study is that the solution of the complete electrode model equations can be very smooth in the interior part of $\Omega$ and that in finite element computations, it is typical that $p$-extensions are very efficient in problems with smooth solutions. For example, when the Poisson equation $\Delta u = f$ in a two-dimensional domain $\Omega$ with zero boundary conditions on $\partial\Omega$ has a smooth solution and uniform mesh refinement is used, the finite element solution $u_h$ satisfies the inequality $\|u - u_h\|_{H^1(\Omega)} \leq Ch_p$, where $h$ is the mesh size, $p$ is the polynomial degree, $C$ is some constant, and $H^1(\Omega)$ denotes the corresponding Sobolev space norm. Since in two dimensions the dimension of the finite element space $N$ grows at the rate $O(p^2/h^2)$, one can deduce from the inequality, that as a function of $N$ the error $\|u - u_h\|_{H^1(\Omega)}$ cannot converge slower in $p$-extensions than in $h$-extensions. For detailed description on $h-$, $p-$ and $hp$-convergence, see Gui and Babuska [4].

## 2. Finite Element Simulation of the Complete Electrode Model

In the complete electrode model, the effective contact impedance between the electrode $e_l$ and the boundary is characterized by the number $z_\ell > 0$. The electrode voltages $U$ induced by the current pattern $I$ can be found by solving the elliptic boundary value problem described by the equation

$$\nabla \cdot (\sigma \nabla u) = 0 \tag{1}$$

in the domain $\Omega$, by the boundary conditions

$$\sigma \frac{\partial u}{\partial n}\Big|_{\partial\Omega \setminus \cup e_\ell} = 0, \quad \int_{e_\ell} \sigma \frac{\partial u}{\partial n}\, dS = I_\ell \quad \text{and} \quad \Big(u + z_\ell \sigma \frac{\partial u}{\partial n}\Big)\Big|_{e_\ell} = U_\ell, \qquad \ell = 1,\, 2,\, \ldots,\, L, \tag{2}$$

on $\partial\Omega$ and by Kirchoff's current and voltage laws $\sum_{\ell=1}^{L} I_\ell = 0$ and $\sum_{\ell=1}^{L} U_\ell = 0$. According to Somersalo *et al.*, [9], with certain assumptions made on the domain and on the conductivity distribution, there exists a unique pair $u \in H^1(\Omega)$ and $U \in \mathbb{R}^L$ that satisfies the weak formulation of this problem. The finite element solution of these equations is the pair

$$u_{FE} = \sum_{i=1}^{N} \alpha_i \varphi_i \quad \text{and} \quad U_{FE} = \sum_{i=1}^{L-1} \beta_i (e_1 - e_{i+1}), \tag{3}$$

where $\varphi_1, \varphi_2, \ldots, \varphi_N$ are the shape functions of the finite element space and $e_1, e_2, \ldots, e_L$ are the standard basis vectors of $\mathbb{R}^L$. The coefficients $\alpha_1, \alpha_2, \ldots, \alpha_N$ and $\beta_1, \beta_2, \ldots, \beta_N$ can be found by solving the linear system of equations $Ax = b$. The entries of the vectors $x$ and $b$ are given by $x_i = \alpha_i$ and $b_i = 0$ if $i \le N$, otherwise $x_i = \beta_{i-N}$ and $b_i = (e_1 - e_{i+1-N})^T I$. The system matrix entries are given by

$$A_{i,j} = \begin{cases} \int_\Omega \sigma \nabla\varphi_i \cdot \nabla\varphi_j \, dxdy + \sum_{\ell=1}^{L} \frac{1}{z_\ell} \int_{e_\ell} \varphi_i \varphi_j \, ds, & \text{if} \quad 1 \le N \quad \text{and} \quad j \le N, \\ -\frac{1}{z_1} \int_{e_1} \varphi_i \, ds + \frac{1}{z_{j+1-N}} \int_{e_{j+1-N}} \varphi_i \, ds, & \text{if} \quad i \le N \quad \text{and} \quad j > N, \\ \frac{1}{z_1} \int_{e_1} ds + \frac{\delta_{i,j}}{z_{j+1-N}} \int_{e_{j+1-N}} ds, & \text{if} \quad i > N \quad \text{and} \quad j > N. \end{cases} \tag{4}$$

where $\delta_{i,j}$ is the Kronecker delta.

## 3. Hierarchic Shape Functions for $p$-extensions

In the standard $p$-version of the finite element method, the shape functions used in $p$-extensions are hierarchic. In this context, the term hierarchic means that the set of shape functions of polynomial order $p$ is in the set of shape functions of order $p+1$, and the number of shape functions which do not vanish at the vertices and the sides of the elements is minimal. Hierarchic shape functions are constructed by using Legendre polynomials

$$P_n(x) = \frac{1}{2^n n!} \frac{d^n}{dx^n} (x^2 - 1)^n, \qquad n = 0, 1, \ldots \quad . \tag{5}$$

Due to the orthogonality properties of these polynomials, hierarchic shape functions are well-suited for computer implementation and have very favorable properties from the point of view of numerical stability [11].

In the one-dimensional case, the standard element is the interval $[-1, 1]$. For this element, the one-dimensional hierarchic shape functions of polynomial order $p$ are defined as

$$N_1(\xi) = \frac{1-\xi}{2}, \quad N_2(\xi) = \frac{1+\xi}{2}, \quad N_n(\xi) = \phi_{n-1}(\xi), \qquad n = 3, 4, \ldots, p+1, \tag{6}$$

where $\phi_n$ is defined as $\phi_n(\xi) = \sqrt{n - 1/2} \int_{-1}^{\xi} P_{n-1}(\xi)\, dt$. These are organized to two categories. The first one is formed by the polynomials $N_1$ and $N_2$, that are called the nodal shape functions, the external shape functions, or the vertex modes. The higher order polynomials $N_3$, $N_4$, $\ldots$, $N_{p+1}$ form the second category. These vanish at the endpoints of the interval $[-1, 1]$ and they are called the bubble functions, the internal shape functions, or the internal modes.

The two-dimensional quadrilateral standard element is the square $[-1, 1] \times [-1, 1]$. The corresponding two-dimensional hierarchical shape functions of polynomial order $p$ are products of one-dimensional shape functions.

$$\begin{aligned} N_{n,m}(\xi,\eta) &= \frac{1}{4}(1+(-1)^n\xi)(1+(-1)^m\eta), && n=1,2, && m=1,2, \\ N^{(0)}_{n,m}(\xi,\eta) &= \phi_n(\xi)\phi_m(\eta), && n=2,3,\dots,p, && m=2,3,\dots,p, \\ N^{(1)}_{n}(\xi,\eta) &= \frac{1}{2}(1-\eta)\phi_n(\xi), && n=2,3,\dots,p, && \\ N^{(2)}_{n}(\xi,\eta) &= \frac{1}{2}(1-\xi)\phi_n(\eta), && n=2,3,\dots,p. && \end{aligned} \tag{7}$$

These are organized to three categories: vertex modes $N_{n,m}$, internal modes $N^{(0)}_{n,m}$, and side modes $N^{(1)}_n$, $N^{(2)}_n$. In this work, only quadrilateral elements are used. Construction of hierarchical shape functions for triangular elements has been described e. g., in [11].

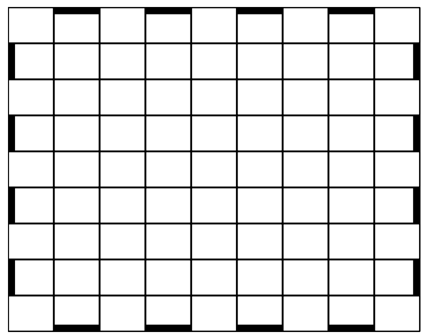

Figure 1: The square shaped domain, the locations of the 16 electrodes, and the coarsest mesh ($h_0 = 1/9$) used in the computations.

## 4. Numerical Experiments

Numerical experiments were performed concerning performances of $h$- and $p$-extensions in FEM simulation of the complete electrode model. In these computations, the domain $\Omega$ was the unit square $[0, 1] \times [0, 1]$ and the conductivity distribution $\sigma$ in $\Omega$ was identically one. Sixteen electrodes with equal contact impedances $z_1 = z_2 = \ldots = z_\ell = 1$ were placed evenly on the boundary (Fig. 1). All the contact impedances were assumed to be equal to one. The generated voltage data constisted of $L-1$ electrode voltage vectors $U^{(1)}, U^{(2)}, \ldots, U^{(L-1)}$ induced by pair drive [7] current patterns $I^{(1)}, I^{(2)}, \ldots, I^{(L-1)}$ such that $I^{(k)}_k = 1$ and $I^{(k)}_{k+1} = -1$ and all other entries are zero. In each of these current patterns, the two current injecting electrodes were located next to each other. The finite element method was used both in data generation and simulation. Each finite element mesh used in these computations consisted of equal-sized square shaped elements as illustrated in Fig. 1. In data simulation, bilinear and hierarchic shape functions were used in $h$- and $p$-extensions, respectively. One $h$-extension process and three $p$-extension processes were executed (Table 1). In these processes, elements of sizes $h = h_0, 2^{-1}h_0, \ldots, 2^{-7}h_0$ with $h_0 = 1/9$ and polynomial orders $p = 1, 2, \ldots, 8$ were employed. The growth of the dimension of the finite element space is reported in Table 1. In data generation, the size and the polynomial order of the elements were $h = 2^{-3}h_0$ and $p = 8$. A vector containing all the generated data is denoted by $\mathbf{U}_{EX}$ and a vector containing the simulated electrode voltages is denoted by $\mathbf{U}_{FE}$. Accuracy of the simulation is measured in $\ell^2$-norm by the relative error

$$\mathrm{RE} = ||\mathbf{U}_{EX} - \mathbf{U}_{FE}||_2/||\mathbf{U}_{EX}||_2. \tag{8}$$

## 5. Results and Discussion

Figure 2 illustrates the convergence of the relative error (8) in the $h$- and $p$-extension processes. The relative error is plotted against the dimension of the finite element space on $\log_{10}$-$\log_{10}$ scale. The results show that $p$-convergence rate is faster than the rate of $h$-convergence.

In finite element computations, $p$-extensions are often motivated by the fact that the solution is smooth whereas $h$-extensions are favorable in the case of non-smooth solutions [11]. According to Evans [3], the interior

Table 1: The executed $h$- and $p$-extension processes: $h$- and $p$-values and finite element space dimensions. In data generation, the size and the polynomial order of the elements were $h = 2^{-3}h_0$ and $p = 8$ (down right corner).

| index | type | $h$-values | $p$-values | finite element space dimensions | | | | | | | |
|---|---|---|---|---|---|---|---|---|---|---|---|
| (a) | $h$ | $h_0, 2^{-1}h_0, \ldots, 2^{-7}h_0$ | 1 | 100 | 361 | 784 | 1369 | 2116 | 3025 | 4096 | 5329 |
| (b) | $p$ | $h_0$ | $1, 2, \ldots, 8$ | 100 | 280 | 460 | 721 | 1063 | 1486 | 1990 | 2575 |
| (c) | $p$ | $2^{-1}h_0$ | $1, 2, \ldots, 8$ | 361 | 1045 | 1729 | 2737 | 4069 | 5725 | 7705 | 10009 |
| (d) | $p$ | $2^{-3}h_0$ | $1, 2, \ldots, 7$ | 1369 | 4033 | 6697 | 10657 | 15913 | 22465 | 30313 | — |

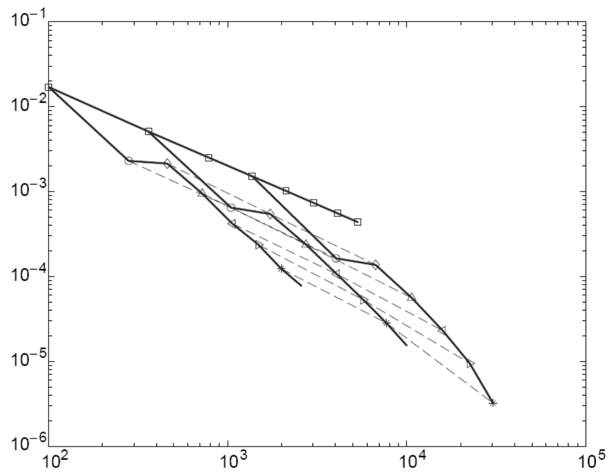


Figure 2: The relative error (8) in the executed $h-$ and $p$-extension processes (a), (b), (c) and (d) plotted against the dimension of the finite element space on $\log_{10}$-$\log_{10}$ scale. The straight line represents the $h$-extension process (a). The three curved lines from left to right represent the $p$-extension processes (b), (c) and (d) respectively. The dashed lines show the $h$-convergence rate in the cases where $p = 2$, 3, 4, 5, 6 or 7.

potential distribution $u \in H^1(\Omega)$ determined by the complete electrode model is smooth provided that the conductivity distribution is smooth. However, it is important to point out that the potential distribution is not smooth in the vicinity of the boundary, since according to the boundary conditions (2) the normal derivative $\partial u/\partial n$ is discontinuous on $\partial\Omega$. Consequently, it is possible that near the boundary the performance of $h$-extensions can be better than that of $p$-extensions. It is also important to note that electrical impedance tomography involves a variety of applications, e. g., detection of tumors, where the conductivity is a non-smooth or a discontinuous function. A local discontinuity in the conductivity distribution, e. g., a tumor, causes local non-smoothness of the interior potential distribution in the vicinity of the discontinuity [3]. This means that the structure of the conductivity can affect the performance of $h$- and $p$-extensions in different parts of the domain. In future work it would be interesting to explore performances of different $hp$-extension processes with different conductivity distributions. For example, whether *a priori* information about the conductivity distribution can be used when designing $hp$-extensions could be an issue in electrical impedance tomography.

From the computational point of view, one important difference in $h$- and $p$-extensions is that in $p$-extensions a lot more computational effort is spent on numerical integration when constructing the system matrix (4) due to the high polynomial order of the shape functions. Electrical impedance tomography involves reconstruction methods, e. g., Markov chain Monte Carlo sampling [6], where efficient forward modeling in terms of computation time is essential, because the forward model equations have to be solved numerous times during the reconstruction process. Another interesting future consideration would be whether there are computationally tractable ways to obtain system matrices needed in EIT reconstruction, e. g., whether *a priori* knowledge about the conductivity distribution can be used when constructing a system matrix.

## 6. Conclusion

In this work, the $p$-version of the finite element method was applied to simulation of the complete electrode model. The motivation for this study was that the solution of the complete electrode model equations can be smooth in the interior domain and that it is typical that the $p$-version is very efficient in problems with smooth solutions. It was shown numerically by using the unit square that the performance of the $p$-version is better than that of the $h$-version when uniform mesh refinement is used. Since the solution of the complete electrode model equations is non-smooth in the vicinity of the boundary, an important topic for the future work is to explore the performance of the $hp$-version of FEM. From the computational point of view, one characteristic difference in $h$- and $p$-versions of FEM is that in $p$-version a lot more computational effort is spent on construction of a system matrix. Another important future consideration is to find computationally tractable ways to obtain system matrices needed in EIT reconstruction. It is also an important issue whether *a priori* knowledge about the conductivity distribution can be used when designing a $p$-FEM implementation to be used in EIT reconstruction.

## Acknowledgment

This work was supported by the Academy of Finland.

### REFERENCES

1. Calderon, A. P., "On an inverse boundary value problem," *Seminar on Numerical Analysis and its Applications to Continuum Physics*, Soc. Brasil. Mat., Rio de Janeiro, 1980.
2. Cheney, M., D. Isaacson, and J. C. Newell, "Electrical impedance tomography," *SIAM Review*, Vol. 41, 85–101, 1999.
3. Evans, L. C., *Partial differential equations*, American Mathematical Society, Rhode Island, 308–316 1998.
4. Gui, W. and I. Babuska, "The h-,p- and hp-versions of the finite elemen method in one dimension. Part I: the error analysis of the p-version. Part II: the error analysis of the h- and hp-versions. Part III: the adaptive hp-version.," *Numerische Mathematik*, Vol. 49, 577–683, 1986.
5. Hartov, A., N. K. Soni, and K. D. Paulsen, "Variation in breast EIT measurements due to menstrual cycle," *Physiological Measurement*, Vol. 25, 295–299, 2004.
6. Kaipio, J. P., V. Kolehmainen, E. Somersalo, and M. Vauhkonen, "Statistical inversion and monte carlo sampling methods in electrical impedance tomography," *Inverse Problems*, Vol. 16, 1487–1522, 2000.
7. Lionheart, W. R. B., J. Kaipio, and C. N. McLeod, "Generalized optimal current patterns and electrical safety in EIT," *Physiol. Meas.*, Vol. 22, 85–90, 2001.
8. Polydorides, N., W. R. B. Lionheard, and H. McCann, "Krylov subspace iterative techniques: on the detection of brain activity with electrical impedance tomography," *IEEE Transactions on Medical Imaging*, Vol. 21, 596–603, 2002.
9. Somersalo, E., M. Cheney, and D. Isaacson, "Existence and uniqueness for electrode models for electric current computed tomography," *SIAM J. Appl. Math.*, Vol. 52, 1023–1040, 1992.
10. Stanley, S. J., R. Mann, and K. Primrose, "Tomographic imaging of fluid mixing in 3-d for single-feed semi-batch operation of a stirred vessel," *Chemical Engineering Research and Design*, Vol. 80, 903–909, 2002.
11. Szabo, B. and I. Babuska, *Finite Element Analysis*, John Wiley & Sons, New York, 1991.
12. Vauhkonen, M., *Electrical Impedance Tomography and Prior Information*, PhD Thesis, University of Kuopio, Kuopio, 1997.
13. Vilhunen, T., L. M. Heikkinen, T. Savolainen, P. J. Vauhkonen, R. Lappalainen, J. P. Kaipio, and M. Vauhkonen, "Detection of faults in resistive coatings with an impedance-tomography-related approach," *Measurement Science and Technology*, Vol. 13, 865–872, 2002.

# The Linear Model for Chirp-Pulse Microwave Computerized Tomography: an Analysis of the Applicability Limitations with an Application to Mammography

**A. M. Massone**
CNR-INFM, Italy

**M. Bertero, M. Piana, and F. Conte**
Universita' di Genova, Italy

**M. Miyakawa**
Niigata University, Japan

Chirp-Pulse Microwave Computerized Tomography (CP-MCT) is a multifrequency imaging modality developed at the Department of Biocybernetics, Niigata University, Niigata, Japan which provides map of temperature variations in biological tissues, via temperature dependence of the attenuation and/or phase constant of the microwave. In a series of papers a linear model for data reduction in CP-MCT has been formulated, whereby a CP-MCT projection is given by a blurred version of the Radon transform of the contrast and the blurring is described by the impulse response of the device. In this talk the applicability limitations of this model will be discussed and the influence of diffraction and refractive effects will be investigated. We will also present the simulation of a mammographycal experiment computed by means of an FD-TD technique and the effectiveness of a reconstruction algorithm based on the linear model will be studied.

# An Improvement of Born Approximation Based on the Linear Sampling Method

**M. Brignone**
Università di Genova, Italy
**M. Piana**
Università di Genova, Italy
**J. Coyle**
Monmouth University, USA

We consider the inverse scattering problem of determining the refractive index of an inhomogeneous body from measurements of the far-field pattern at fixed frequency. Under Born approximation conditions this problem can be reduced to a Fourier transform inversion problem with limited data. In this talk we describe a reconstruction approach where the linear sampling method is applied to obtain a priori information on the support of the scatterer and an out-of-band extrapolation procedure is performed by means of a projected iterative algorithm. Applications to two-dimensional examples show that this approach may provide notable super-resolution effects.

# Computational Validation of a Particle Filtering Approach to the Solution of the Magnetoencephalography (MEG) Inverse Problem

**A. Sorrentino and M. Piana**
Università di Genova, Italy

The problem of estimating the parameters of a source dipole from dynamical measurements of the magnetic field in a simulated magnetoencephalography (MEG) experiment is addressed by means of a Bayesian approach computed with a particle filtering technique. In particular, we validate this method in the presence of volume currents and accounting for the neuronal origin of the noise affecting the measurements. The effect of encoding a priori information in the prior density distribution function is also tested.

# Resolution and the Linear Sampling Method

**J. Coyle**
Monmouth University, USA

**R. Aramini**
Universitá di Trento, Italy

The linear sampling method (LSM) is a visualization scheme for frequency domain inverse problems that provides an image of the profile of the scatterer. In particular, the method consist of plotting the norm of a regularized solution, $g$, to a linear Fredholm equation of the first kind at points in a grid that cover a region where the unknown scatterer is thought to be located. The profile of the scatterer is then characterized by the fact that the norm of $g$ increases without bound as the sampling points approach the boundary of the scatterer. A tremendous advantage of the LSM is that it is not computationally expensive to implement and no a priori knowledge of the physical traits of the scatterer are needed. It is, however, the case that several questions remain regarding the choice of sampling grid and the effects on the resolution of the profile. This talk will focus on both illustrating the difficulties that one may encounter as well as offer possible solutions to this problem.

# Robust Design of the Field in Medical Electromagnetic Systems

**P. Lamberti**, **G. Spagnuolo**, **and V. Tucci**
University of Salerno, Italy

The field uniformity in a region as large as possible plays a great role in the design of medical electromagnetic systems, in the case both of Magnetic Resonance Imaging (MRI) and Electron Paramagnetic Resonance (EPR). However the inevitable uncertainty and tolerance on the design parameter due to the component derive and manufacturing processes can lead the system to work in an unexpected range of field value and with low uniformity. The field robustness in presence of that variation can be obtained performing a nominal system design that guarantees the operation in a low field sensitivity region of the parameter space.

In this paper we introduce a robust design approach based on Interval Analysis (IA) and Finite Element Method (FEM). In particular we show the using of FEM in conjunction to the Design of Experiment to obtain a $v$-variate polynomial expression of the field in the centre of the working volume as a function of the parameter $f(x_1, x_2, \ldots, x_v)$, where $v$ is the number of parameter design. The robustness analysis of such polynomial function by means of the IA allows to select a region of low field variability in the parameter space, i.e. the robust nominal design $(x_{10}, x_{20}, \ldots, x_{v0})$ respect to a variation of $\pm\delta_i$ around each parameter nominal value. The robustness of a solution is obtained looking to the width of the complete Taylor series of the polynomial function around the nominal solution while the real variables, i.e., the $v$ parameter design, and the real operations are substituted respectively with interval variables and operations. Such interval variables $X_i = [x_{i0} - \delta_i, x_{i0} + \delta_i]$, for $i = 1, \ldots, v$, are symmetric intervals, centred in the correspondent parameter nominal values $(x_{10}, x_{20}, \ldots, x_{v0})$ and with radius of variation equal to the particular variations $\delta_i$.

In this paper an example of the proposed approach at the design of an EPR is reported while the robustness is checked by means of a Monte Carlo analysis.

# A Class of Non-iterative Methods Applied to Microwave Tomography at a Fixed Frequency

**H. Haddar**
INRIA Rocquencourt, France

The imaging problem at study consists into finding the location and the shape of inhomogeneous and possibly anisotropic inclusions embedded into a homogeneous medium from electromagnetic measurements at a fixed frequency. We consider the cases where the wavelength is of the same order of magnitude as the inhomogeneities size. We shall investigate imaging techniques based on the sampling method formalism: the inhomogeneities are visualized by constructing an indicator function whose evaluation at a given point (sampling point) requires to solve an ill posed linear problem.

The first one is the classical linear sampling method that requires the computation of the Green tensor for the background medium, which may turn out to be numerically very costly, even for simple configurations where analytical expressions can be derived. The second one is an alternative approach based on the reciprocity gap functional [2, 1] that avoids the computation of this tensor. However, it requires the knowledge of both the electric and magnetic field at a given surface. This method is also shown to have a more general setting than the linear sampling method, allowing for instance a large flexibility in the choice of the indicator function. This choice can be exploited to enhance the performance of the method if some a priori information is known about the type of inhomogeneities.

The numerical efficiency and limitations of both methods will be discussed in the talk.

# Time-domain Image Reconstruction in an Experimental Prototype for Breast Cancer Detection

**A. Fhager**, **P. Hashemzadeh**, **and M. Persson**
Chalmers University of Technology, Sweden

Microwave tomography is rapidly developing into a promising imaging technique that could be useful in many different applications where a non-invasive detection of internal dielectric properties is required. Such a technique could be very useful in mammographical imaging in the search for breast cancer tumours. There is a considerable benefit in using microwaves in the diagnosis of breast cancer tumours due to a significant contrast in the dielectric properties between tumour and surrounding tissue compared to $X$-rays where the contrast could be as low as a few percent.

We have developed an experimental prototype of an electromagnetic tomographic system for microwave imaging of the breast together with a time-domain conjugate-gradient image reconstruction algorithm. The FDTD formulation is used to model the electromagnetic problem and for solving the forward scattering problem. The inverse problem is solved iteratively by minimising a cost functional containing the difference between the measured scattered field and the corresponding simulated field. Gradients are computed from solutions of the adjoint Maxwell equations and a line search is made to find the minimum of the functional. The measurements are made using a circular array of dipole antennas and conducted in frequency domain. Time-domain signals are synthesised by means of an inverse Fourier transform.

In this paper we present our latest advances on optimising the resolving capabilities and accuracy in the reconstructed image. This includes both experimental and algorithmic issues. We also evaluate the performance of the imaging method by reconstruction of tissue like phantom objects.